

Altitude determination of ultraviolet measurements made by the Student Nitric Oxide Explorer

A. W. Merkel¹ and C. A. Barth¹

¹Laboratory for Atmospheric and Space Physics, University of Colorado, Boulder, Colorado, USA

S. M. Bailey²

²Center for Atmospheric Sciences, Hampton University, Hampton, Virginia, USA

Abstract. The spinning motion of the Student Nitric Oxide Explorer spacecraft allows for the measurement of limb profiles of atmospheric radiation. In order to interpret the observations an accurate altitude reading is necessary. Included in the limb profile is Rayleigh-scattered solar radiation that can be used to determine altitude. The Rayleigh profile increases exponentially with decreasing altitude until the absorption due to ozone dominates the shape, producing a peak near 53 km. We use the Rayleigh scattering peak to register the measured profile in altitude for each ultraviolet spectrometer observation. A single-scattering radiance model is developed and used to provide an altitude-dependent shape of the Rayleigh profile. The altitude registration is done by correlating the data to the model for each measured profile. By systematically shifting the measured profile in small increments and fitting the shifted profile to the model the quality of the fit is determined. The shifted profile that best correlates with the model profile determines the correct shift in altitude to 1.5 km precision.

1. Introduction

There are a number of methods for determining the attitude of a spacecraft, all of which require an instrument for sensing the angular orientation of the spacecraft coordinates with respect to some external reference such as the Sun, the stars, or the magnetic field or horizon of a planet. Measuring instruments include magnetometers, Global Positioning Systems (GPSs), Sun or star sensors, and horizon-crossing indicators (HCIs). Although all have positive attributes, inexpensive small satellites commonly utilize HCIs, which are infrared instruments that detect the contrast between the cold of deep space and the heat of the Earth's atmosphere [Larson *et al.*, 1992]. The Student Nitric Oxide Explorer (SNOE) satellite utilizes HCIs for attitude determination. This paper will show that in addition to HCIs a measurement of the ultraviolet limb profile can be used to determine attitude information.

The HCIs on SNOE are used to provide positioning information for attitude control and to initiate timing signals for the science payload. On low Earth-orbiting, spinning spacecraft, horizon detection allows for the determination of pitch and roll axes as well as spin period. The HCI limb pulses initiate a programmable timer, set to enable data storage during the desired portion of the spacecraft spin period. The delay initiated by the HCIs is set such that the ultraviolet spectrometer (UVS), which is designed to measure atmospheric emissions when viewing the limb of the Earth, starts storing data when the instrument line of sight intersects the 200 km tangent altitude on the limb. However, the accuracy of the pointing based on the HCI trigger pulse is $\pm 0.5^\circ$,

which is $\sim \pm 20$ km on the limb, based on the orbital altitude of the SNOE spacecraft. The uncertainty is caused by the variability of the infrared limb with altitude and latitude, detector noise, the finite field of view of the HCIs, and spin period variability. Although this uncertainty is acceptable for SNOE's attitude determination, it is not sufficient for analysis of the UVS limb profiles, which need a higher precision in altitude. Our goal is to determine the altitude to a precision of 1.5 km, which is one half the image of the slit on the horizon.

The UVS was designed to measure fluorescent scattering of sunlight by nitric oxide (NO) at 215.0 and 236.5 nm. The global NO variation will be presented by C.A. Barth *et al.* (manuscript in preparation, 2001). Along with emissions from NO the limb profile includes emissions due to Rayleigh-scattered solar radiation. The limb profile of Rayleigh-scattered photons has a distinct altitude-dependent shape, which includes a peak in the signal at a stable altitude. The Rayleigh-scattering measurement can be used as a postobservation calibration of limb-crossing data. The measured profile can be recreated with a single-scattering radiance model. By comparing the measured limb profiles to model profiles we can accurately determine the altitude range measured, independent of the HCIs.

2. Spacecraft and Instrument Description

The SNOE spacecraft was launched in February of 1998 to make global observations of NO and the sources of energy that produce it [Solomon *et al.*, 1996; Bailey *et al.*, 1996]. SNOE is in a circular, near-polar, Sun-synchronous orbit that provides almost complete latitudinal coverage from 80°S to 80°N and at an altitude of 556 km with its ascending node at 1030 A.M./P.M. LT and an orbital period of 96 min. In addition, the spacecraft is spinning with a period of 12 s. During each downward scan of

Copyright 2001 by the American Geophysical Union.

Paper number 2001JA001111.
0148-0227/01/2001JA001111\$09.00

Table 1. Instrument Parameters

Feature	Parameter
<i>Telescope</i>	
Mirror system	single mirror, off-axis paraboloid
Off-axis angle	15°
Focal length	250 mm
Focal ratio	<i>f</i> /5
Effective collection area	20.7 cm ²
Material	fused silica
Coating	aluminum, MgF overcoat
Field of view	0.071° x 0.75°
<i>Spectrometer</i>	
Mounting	Ebert-Fastie
Focal length	125 mm
Focal ratio	<i>f</i> /5 (zero order)
Wavelength coverage	channel 1: 215.0 nm channel 2: 236.5 nm
Grating	frequency: 3600 g mm ⁻¹ (plane) blaze: 25°36'
Wavelength bandpass	channel 1: 3.8 nm channel 2: 3.7 nm
Wavelength dispersion	1.8 nm mm ⁻¹
Entrance slit	0.31 mm x 3.2 mm
Exit slit	2 mm x 4 mm
Grating angle	22.7° (to slit plane)
Exit slit separation	10.8 nm

the Earth's limb the UVS is programmed to record 65 samples at 2.4 ms per sample. The UVS measures NO on two different wavelength channels centered at 215.0 and 236.5 nm. The observational vertical resolution, as set by the width of the entrance slit, is 3.2 km on the Earth's limb. SNOE moves ~0.75° along its orbit each spin. By averaging six consecutive spins the horizontal resolution is about 5° in latitude. The UVS atmospheric data products are routinely indexed on a standard 5° latitude grid and 3.33 km altitude grid.

The SNOE UVS design is a modification of the ultraviolet spectrometer flown on Solar Mesosphere Explorer (SME) [Rusch *et al.*, 1984]. Instrument parameters are listed in Table 1. The telescope is a single-element, *f*/5, off-axis paraboloid with a 250 mm focal length. The telescope images the spectrometer entrance slit onto the Earth's limb with the long axis of the slit parallel to the horizon. The slit's projected size is 3.2 km (0.071°) perpendicular to the limb and 35 km (0.75°) parallel to the limb. The spectrometer is an Ebert-Fastie design with *f*/5, 125 mm focal length concave mirror, and a fixed plane grating. The spectrometer configuration is designed to center 215.0 and 236.5 nm onto two photomultiplier detectors (one band per detector). To ensure that the desired wavelengths fall on the detectors, the exit slits were designed to have a 3.6 nm bandpass (full width at half maximum). The wavelength separation of the two channels is 10.8 nm. The detectors are Hamamatsu R759 F photomultiplier tubes with pulse-counting electronics. Both detectors have a fused silica window and a cesium telluride photocathode and are thus sensitive to radiation between 150 and 300 nm.

The HCIs were developed to be sensitive to infrared radiation between 14 and 16 μm emitted by carbon dioxide (CO₂) from the Earth's atmosphere. A & M Associates produced the HCIs. The SNOE spacecraft has two HCIs in a V pair configuration, which are used to detect the roll and pitch reference horizon. The HCIs have a field of view of 2° (vertical) by 5° (horizontal). Infrared

radiation is focused onto the pyroelectric detector by a thallium bromide lens. The focal length of the collecting lens allows the image in the field of view to fit on the 1 mm diameter of the detector. The collected radiation passes through a wideband interference germanium filter with a bandwidth of 2.3 μm. The filter protects the detector from potential damage when exposed to direct visible and near-infrared solar radiation. It also eliminates effects due to reflected sunlight from the Earth and clouds as well as most of the thermal radiation from water vapor. The filter transmits radiation from 14 to 16 μm onto the pyroelectric detector, which in turn responds to changes in the level of radiation. When viewing radially from the spinning spacecraft, the detector senses a rapid change of the light level when crossing the horizon from cold space to warm Earth.

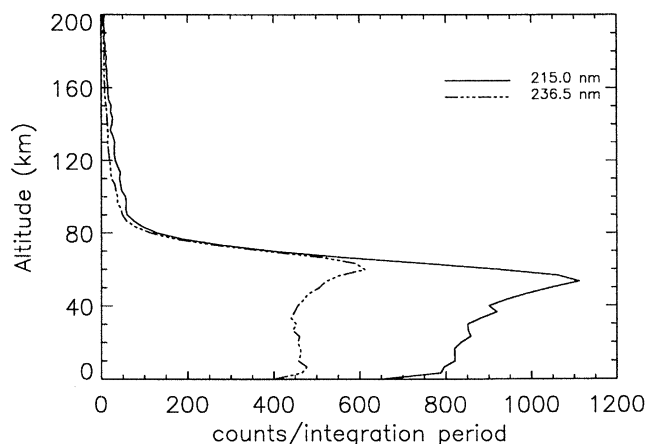


Figure 1. UVS measured profiles of the 215.0 and 236.5 nm channels on day 350 of 1998 at the equator.

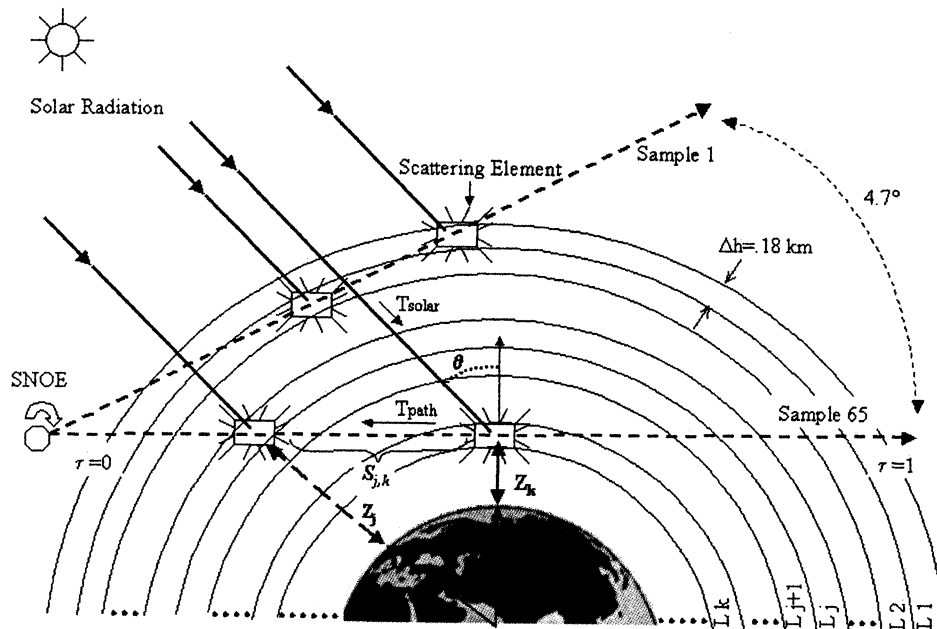


Figure 2. The limb-scanning geometry for SNOE. As SNOE spins with a 12 s period, the UVS takes 65 samples along the limb covering 4.7°. The model includes the path of the solar photon (T_{solar}) to the scatter point and the path of the scattered photon to the instrument (T_{path}). The atmosphere is split into onion skin shells in steps of 0.18 km.

3. Observations

The HCIs on SNOE trigger off of the infrared signal emitted by CO_2 and in turn provide a timing fiducial for the spacecraft. When the HCI's field of view intersects the Earth's horizon, it sends a pulse to the instrument electronics. Once the pulse has been received, the instrument waits a specified delay period before storing data. This timing device is set such that the UVS will start storing data when it is looking at the limb. The HCIs on SNOE are set to trigger at a tangent altitude of 40 km. Ideally, the UVS will store data at the same altitude each spin. The measured altitude range can be determined by simple trigonometry and known timing components. However, on SNOE the HCIs could have up to ± 20 km error because of a combination of the field of view and noise of the HCI detectors' spin period variability and the variation of the CO_2 with season and latitude. Since the delay remains constant, the HCI triggering error causes the UVS to store data for different altitude ranges for each scan. The altitude range for each scan must be determined to analyze properly the UVS data.

SME, a very similar spacecraft, used HCIs as its primary altitude determination technique. The HCIs on SME also had a large uncertainty; however, their technique for registering altitude for the limb profiles measured from SME's UVS was based on the IR trigger altitude. Cowley and Lawrence [1983] modeled the HCI trigger altitude, which occurs at the maximum slope of the IR radiance signal. This model incorporated the effects of seasonal and latitudinal variation of CO_2 , as well as satellite orbit and spin geometry. With an accurate determination of the HCI trigger altitude the altitude registration of the limb profile is also determined. SME's limb altitude registration is quoted to have an accuracy of 1 km.

Instead of modeling the HCI trigger altitude and then relating it to the measured data as SME did, we used the science data directly to register altitude. The true altitude range of the measured UV limb profile is determined by comparing UVS data to model

predictions of limb profiles of Rayleigh-scattered ultraviolet solar radiation. Altitude-dependent concentrations of nitrogen, oxygen, and ozone molecules are inputs to the model and are provided by empirical models [Hedin, 1991; Keating *et al.*, 1990]. By comparing the altitude at which the Rayleigh-scattered radiance model and the measured profile reach a maximum the altitude profile for the data can be determined.

4. Model Description

The UVS measures altitude profiles of Rayleigh-scattered solar photons in the 215.0 and 236.5 nm spectral region, as well as NO emissions. The shape of the limb profile of Rayleigh scattering is altitude-dependent; therefore the profile provides altitude information and can be used to determine precisely where the UVS is pointing when it stores data. Figure 1 illustrates a typical UVS limb profile for the 215.0 and 236.5 nm channels. Within the altitude range measured several distinct features can be identified in the profiles. Between 170 and 90 km the UVS measures the daytime airglow emissions from NO. Below 90 km, Rayleigh scattering of sunlight off of air molecules becomes brighter than the NO airglow emissions. Therefore the radiance scattered increases exponentially with decreasing altitude until the absorption due to ozone and molecular oxygen diminish it. The radiance reaches a maximum at the same altitude the optical depth of ozone along the line of sight becomes $\tau \approx 1$. The altitude of the maximum depends on the ozone cross section and the integral number of ozone molecules along the path. This altitude is different for the two wavelengths measured by the UVS.

To model the radiance, it is convenient to split the atmosphere into "onion skin" shells. It is assumed that each small concentric spherical shell has a constant density. As mentioned above, the UVS typically takes 65 samples as it scans through the atmosphere. Figure 2 illustrates the UVS limb-viewing geometry. At each altitude sampled the UVS line of sight intersects a number of onion skin shells to the tangent altitude. The altitudes sampled

are in 3.33 km steps (about half the scale height at this altitude region). In order to assume each shell has a constant volume density of molecular nitrogen, molecular oxygen, and ozone the shell widths are split into steps of 0.18 km. As illustrated in Figure 2, the number of shells intersected along the line of sight to the tangent altitude depends on the altitude being sampled because the number of shells intersected increases with decreasing altitude. This geometry creates a lower triangular matrix.

The radiance is a direct measurement of the integral number of scatterers and absorbers along the instrument line of sight to each tangent altitude. The equation used to model the Rayleigh-scattered radiance is

$$4\pi I_\lambda = F_\lambda \sigma_\lambda P(\Theta) \Delta\lambda \int_{-\infty}^{\text{UVS}} N[z(s)] T_{\text{path}}(s) T_{\text{solar}}(s) ds. \quad (1)$$

The modeled radiance I_λ is determined by F_λ , the solar flux at wavelength λ ; σ_λ , the Rayleigh-scattering cross section; $P(\Theta)$, the Rayleigh phase function, and $N[z(s)]$, the volume density of scatterers at altitude z . The solar flux at wavelength λ is provided by data from the Upper Atmosphere Research Satellite (UARS) Solar Stellar Irradiance Comparison Experiment (SOLSTICE) [Woods *et al.*, 1996]. The integration is along the line of sight S . In order to compare with the observed limb profile the modeled radiance is multiplied by the spectral bandpass $\Delta\lambda$ (see Table 1). The Rayleigh phase function describes the probability that polarized light will scatter in the direction of the scattering angle Θ [e.g., see, Thomas and Stannnes, 1999] given by

$$P(\theta) = \frac{3}{4}(1 + \cos^2 \theta). \quad (2)$$

This function is normalized to 4π when integrated over all scattering angles. The extinction of the radiance along the line of sight is represented by the transmission. The transmission from the Sun to the scatter point is represented by T_{solar} . The transmission from the scattering point to the UVS is represented by T_{path} . The transmission depends on the optical depth through each constituent considered as described by

$$\begin{aligned} T_{\text{path}}(s) &= \exp[-\tau_{\text{sca}}^{\text{path}}(s) - \tau_{\text{ozone}}^{\text{path}}(s) - \tau_{\text{O}_2}^{\text{path}}(s)] \\ T_{\text{solar}}(s) &= \exp[-\tau_{\text{sca}}^{\text{solar}}(s) - \tau_{\text{ozone}}^{\text{solar}}(s) - \tau_{\text{O}_2}^{\text{solar}}(s)] \end{aligned} \quad (3)$$

The optical depth along the path, τ^{path} , is an integral along $S_{j,k}$, the line of sight of the instrument, as described by

$$\begin{aligned} \tau_{\text{sca}}^{\text{path}}(s) &= \sigma_{\lambda,\text{sca}} \int_j^k N[z(s_{j,k})] ds_{j,k}, \quad \sigma_{\lambda,\text{sca},215.0\text{nm}} = 2.54e^{-25} \text{cm}^2 \\ \tau_{\text{ozone}}^{\text{path}}(s) &= \sigma_{\lambda,\text{abs}}(o_3) \int_j^k O_3[z(s_{j,k})] ds_{j,k}, \quad \sigma_{\lambda,\text{abs}O_3,215.0\text{nm}} = 1.04e^{-18} \text{cm}^2 \\ \tau_{\text{O}_2}^{\text{path}}(s) &= \sigma_{\lambda,\text{abs}}(o_2) \int_j^k O_2[z(s_{j,k})] ds_{j,k}, \quad \sigma_{\lambda,\text{abs}O_2,215.0\text{nm}} = 5.59e^{-24} \text{cm}^2 \end{aligned} \quad (4)$$

where the values of the cross sections are taken from DeMore *et al.*, [1997] and Bates [1984]. The length of the path, $ds_{j,k}$, through each onion skin shell is calculated by

$$ds_{j,k} = [(Re + Z_j)^2 - (Re + Z_k)^2]^{1/2} - S_{j+1,k}, \quad (5)$$

where Re is the radius of the Earth (see Figure 2). The path length is multiplied by the volume density within the j th shell and inte-

grated along the line of sight. We will call this product the slant column density. The slant column density represents the total density for each constituent encountered along the path. The larger the slant column density encountered, the higher the probability that the incident radiation will be scattered or absorbed out of the path. To determine the optical depth τ , the slant column density is multiplied by a wavelength-dependent absorption or Rayleigh-scattering cross section. The optical depth is determined for each constituent contributing to the extinction of the radiance. All contribute to the total transmission along the path of radiation. The use of a single-scattering approximation is justified at the wavelengths considered because the slant optical depths due to Rayleigh scattering are $\ll 1$ at 53 km. The vertical optical depth due to ozone absorption is approaching 1 and is > 1 at lower altitudes and therefore eliminates a contribution from the Earth.

The optical depth along the solar incident path τ^{solar} , in (6), is integrated along the path of the Sun to the scatter point:

$$\begin{aligned} \tau_{\text{sca}}^{\text{solar}}(s) &= \sigma_{\lambda,\text{sca}} Ch(\theta) \int_{z_0}^z N[z] dz \\ \tau_{\text{ozone}}^{\text{solar}}(s) &= \sigma_{\lambda,\text{abs}}(o_3) Ch(\theta) \int_{z_0}^z O_3[z] dz \\ \tau_{\text{O}_2}^{\text{solar}}(s) &= \sigma_{\lambda,\text{abs}}(o_2) Ch(\theta) \int_{z_0}^z O_2[z] dz \end{aligned} \quad (6)$$

The direction of the incident radiation is inclined from the zenith creating a slant path. The angle between the incident radiation and the zenith is the solar zenith angle θ (see Figure 2). The incident radiation is attenuated along the slant path. The attenuation of the solar irradiance increases with increasing solar zenith angle. To calculate the slant column density, the volume density along the vertical path is integrated and multiplied by the Chapman function $Ch(\theta)$. The Chapman function is defined as the ratio of the slant column density N along the incident path to the vertical column density N_v . It accounts for the attenuation of the solar flux due to the slant path. The function [Chapman, 1931] is described by

$$Ch(\theta, R_o/H) \equiv \frac{N(R_o, \theta)}{N_v(R_o)}. \quad (7)$$

Although there are many good approximations for the Chapman function, the analysis by Fitzmaurice [1964] leads to a convenient expansion for computing purposes. This Chapman approximation, for zenith angles $\leq 90^\circ$, is given by

$$\begin{aligned} \sqrt{\pi X/2} \exp S \{1 - \text{erf} \sqrt{S}\}, \quad S < 9.5, \\ \sec \theta \left\{ 1 - \frac{1}{2S} + \frac{3}{4S^2} - \frac{15}{8S^3} \right\}, \quad S \geq 9.5, \end{aligned} \quad (8)$$

where

$$S = X \cos^2(\theta/2).$$

$$X = (Re + Z)/H. \quad (9)$$

The approximation depends on the radius of the Earth, Re ; the altitude of observation, Z ; the scale height H at altitude of observation; and the solar zenith angle θ .

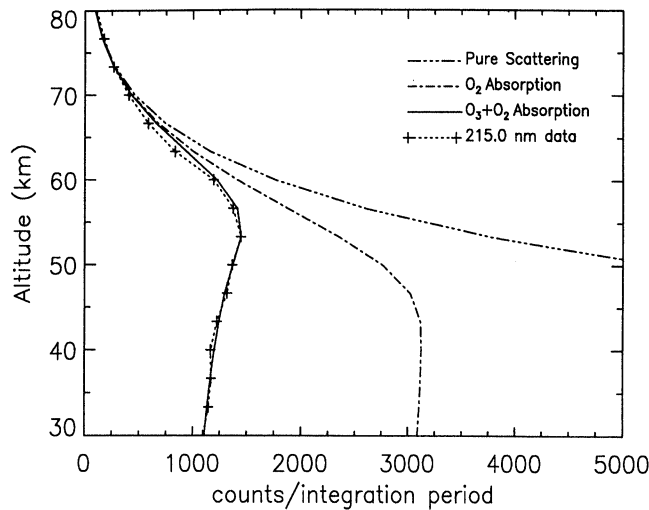


Figure 3. Comparison of Rayleigh-scattering profiles for three cases. The dash-three-dotted line shows the Rayleigh profile with the effects of pure scattering included. The dash-dotted line shows the Rayleigh profile with both pure scattering and the absorption due to molecular oxygen included. The solid line shows the Rayleigh profile with pure scattering, the absorption due to molecular oxygen, and the absorption due to ozone included. The plus-dotted line is UVS data for channel 215.0 nm on day 350 of 1998 at the equator.

The above calculation requires two different atmospheric models as inputs. The altitude-dependent volume densities $N_2[z]$ and $O_2[z]$ are provided by the Mass Spectrometer Incoherent Scatter (MSIS) model [Hedin, 1991]. The outputs of temperature and number density are dependent on the time, altitude, latitude, and longitude. Currently, the Committee on Space Research (COSPAR) International Reference Atmosphere: 1986 model provides the ozone prediction. The COSPAR reference includes monthly latitudinal variations based on ozone data from multiple satellite experiments [Keating *et al.*, 1990] and provides mixing ratios (ppmv) on a pressure grid (mbar) for an average day of each month. To be consistent with the model inputs, the COSPAR values are converted to number density (cm^{-3}), put on a 3.33 km altitude grid, and interpolated to have values for every day of the year.

Figure 3 shows the results of the process described above. The peak and magnitude of the maximum of the radiance profile depend mainly on the volume density of ozone. The dependence on ozone is best demonstrated by the progression in Figure 3. If the model only included the effects of scattering, the signal would exponentially increase without attenuation. However, at the wavelengths measured, absorption from molecular oxygen and ozone is the main source of extinction and needs to be included. Figure 3 illustrates that the absorption due to molecular oxygen slightly changes the signal profile. However, by including the absorption due to ozone the radiance profile is modified significantly, and the signal decreases by a factor of 3 below 80 km, inducing a peak. Included in Figure 3 are data from the 215.0 nm channel measured on day 350 in 1998 at the equator illustrating a good match between data and model. Since the peak depends strongly on the concentration of ozone, the vertical volume density of ozone is the largest cause of uncertainty in the model. It is important that the uncertainties in the model are small and that the altitude of the peak is stable. The questions then arise of the

accuracy of the COSPAR 1986 ozone model relative to other improved models and interannual variations and how an uncertainty in ozone vertical density will affect the altitude of the peak.

5. Model Uncertainties

When analyzing the uncertainty in the vertical ozone profile, we are only concerned with mesospheric ozone, ranging from 53 to 70 km. Because the peak of the Rayleigh profile is produced when the slant optical depth of ozone is near 1, only the altitudes along the line of sight to the tangent altitude of the Rayleigh peak contribute to the slant optical depth. At this altitude range the COSPAR 1986 ozone model is constrained by measurements from SME's UVS and IR instruments. Rusch *et al.* [1984] and Thomas *et al.* [1984] describe the error analysis for these two instruments in great detail. The combined standard deviation of these measurements presented in the reference model is 10%. In 1996, *Advances in Space Research* released an improved ozone reference model for the COSPAR international reference atmosphere [Keating *et al.*, 1996]. The improved reference model utilized reprocessed data from the same satellite experiments used in the 1986 model. The reprocessed SME ozone data (with the same instrument uncertainties) indicate a 7% decrease from the SME data currently being used in the Rayleigh-scattering model. Wang *et al.* [1999] presented a reference model for middle atmospheric ozone using recent measurements from the Stratospheric Aerosol and Gas Experiment (SAGE), the Halogen Occultation Experiment (HALOE), and the Microwave Limb Sounder (MLS). This model analysis reported to have differences up to 10% from the Keating *et al.* [1996] results and a model accuracy of $\sim 5\%$ for the appropriate altitude range. All three reference models provide a zonal mean for each month for a 1 year period and indicate an interannual variability of $<4\%$. We assume that the accuracy of the COSPAR 1986 reference model is the RMS total from all described resources, $\sim 17\%$. Figure 4 incorporates an uncertainty in ozone of 20% and shows an altitude change of the Rayleigh peak of only 1 km. Therefore, by including known sources of error to the utilized ozone model the uncertainty in the altitude profile due to ozone is 1 km.

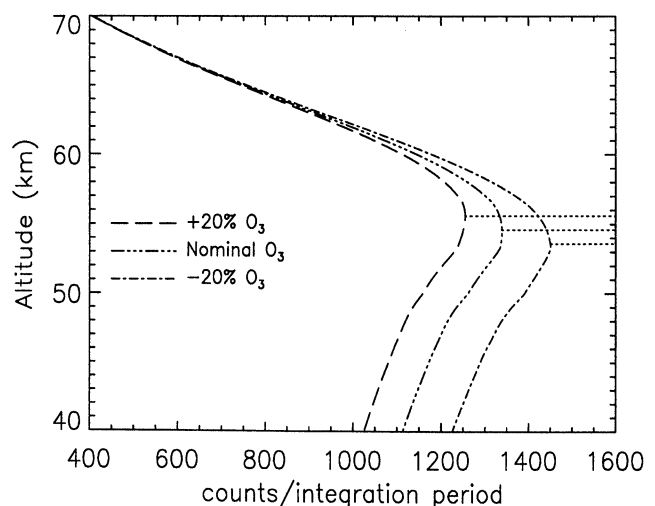


Figure 4. Model calculation with a $\pm 20\%$ change in ozone. A 20% change in ozone changes the altitude of the Rayleigh-scattering peak by 1 km.

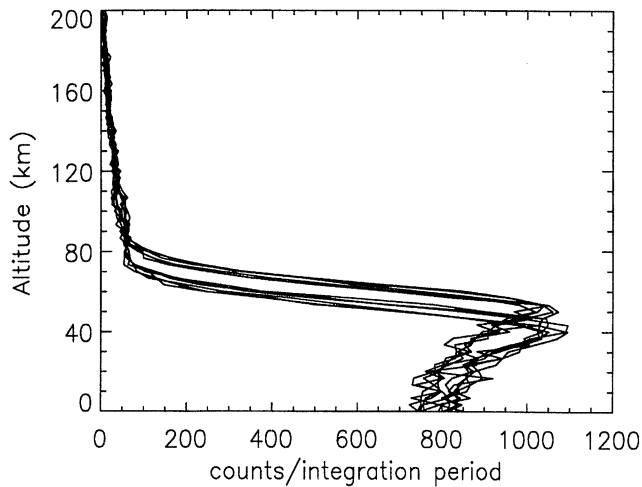


Figure 5. Raw UVS data profiles for 10 consecutive spins illustrate the variability of the altitude registration determined by the HCIs from spin to spin.

Thermospheric nitric oxide may affect the Rayleigh-scattering peak through either emission or absorption. The contribution to the Rayleigh-scattering signal from NO emissions at 106 km for the spectral bandpass measured is small compared to the contribution from Rayleigh scattering and ozone absorption at 53 km. Their relative brightness is shown in Figure 5. The contribution from NO absorption can be estimated by calculating the line width of the absorption feature. The Doppler line width of a single rotational NO line is 4.0×10^{-4} nm at 200°K. In the spectral bandpass of 3.8 nm, centered on 215.0 nm, there are ~ 200 rotational lines for a total effective line width of 8.0×10^{-2} nm [Eparvier and Barth, 1992]. If there were sufficient NO in the thermosphere to absorb all of the Rayleigh-scattered radiance in the total effective line width for NO, only 8.0×10^{-2} nm / 3.8 nm = 2% of the Rayleigh-scattered radiance would be absorbed. This 2% attenuation is nearly constant with the change in line of sight and therefore is only a linear scaling factor and does not affect the altitude registration.

The UVS detects polar mesospheric clouds (PMC) in both channels (see Figure 9) in the polar mesosphere, 3 months out of the year, centered on summer solstice in each hemisphere. Therefore 12% of the total UVS limb observations may have detected scattering from a PMC. It is important to know what the effect of PMC scatter in the line of sight has on the altitude registration. When referring to PMC brightness, a commonly used term is scattering ratio (SR), which is the ratio of PMC brightness to an average Rayleigh background in counts at 83 km. The brightness of a PMC in the UVS limb observations directly depends on the observed scattering angle. Ice particles scatter light more efficiently in the forward direction than in the backward direction. Because of the orientation of the SNOE orbit, all PMCs observed in the Northern Hemisphere are due to backward scattered photons, and all PMCs observed in the south are due to forward scattered photons. Therefore, on average, PMCs observed from SNOE will have larger SR in the south than in the north. Figure 6 illustrates a modeled Rayleigh profile including a very basic modeled PMC with different SR values. Referencing Figure 6, the Rayleigh peak altitude only moves ~ 0.5 km with a SR of 20. In the north, 100% of observed clouds, and in the south, 95% of observed clouds have SR of 20 and less. Therefore an uncertainty

of 0.5 km is included because of PMC scatter in the field of view. Because the uncertainty is small, we allow for the possibility of a PMC occurrence throughout the year and always include it. In $\sim 1\%$ of the cloud observations the SR is much greater than 20 (i.e., SR = 50 - 100). In these cases the profiles are not used in the NO analysis.

6. Altitude Determination

It is known from the model analysis that the shape of the Rayleigh-scattered radiance profile is altitude-dependent and the altitude of the peak is wavelength-dependent (see Figure 1). However, since both channels are storing data simultaneously, only the 215.0 nm channel is needed to determine the altitude scale, and the 236.5 nm channel is corrected by the same amount. The HCI delay is calculated to try to position the radiance maximum near 53 km for the 215.0 nm channel. Figure 5 illustrates raw unprocessed UVS data versus altitude for 10 consecutive spins. By plotting the 65 samples measured per spin on a standard 3.33 km altitude grid from 200 to 0 km the altitude at which the radiance reaches a maximum is not consistently 53 km. To get the data onto the desired altitude grid, the data must be shifted by a determined amount to position the radiance peak at the correct altitude.

The process of eliminating the uncertainty in altitude registration due to the HCI errors begins with an initial shift to position the peak altitude at 53 km. This is an initial shift because the altitude of the peak is not exactly at 53 km since it varies with ozone concentration, which varies with latitude and season of the year. The initial shift will position the peak near the true altitude to within a few kilometers. Figure 7 is a histogram of the initial altitude shift for each UVS profile for 1 year of operations (about one million observations). The full width at half maximum of the histogram indicates the HCIs have a ± 20 km error in altitude registration. This is consistent with the HCI trigger altitude variation caused by the field of view and noise of the HCI detector, the spin variability, and the variation of the CO₂ with season and latitude as discussed in Section 3. Even though these errors are large, this initial shift eliminates their contribution from the data processing.

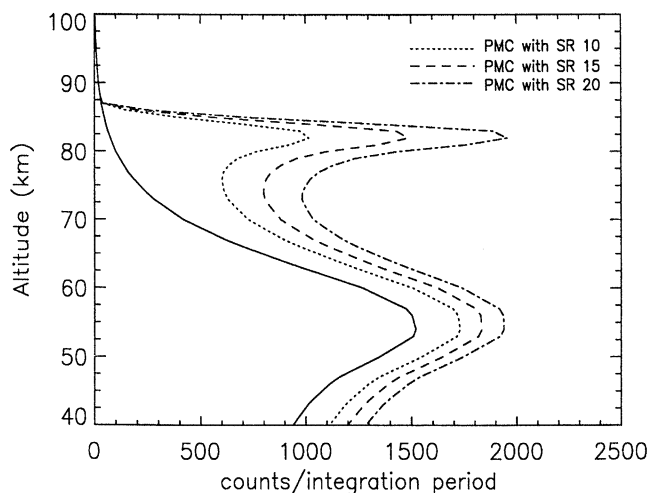


Figure 6. Model calculation with a modeled PMC included. The solid line is an average Rayleigh-scattering profile. Each additional line includes a PMC with increasing scattering ratio (SR).

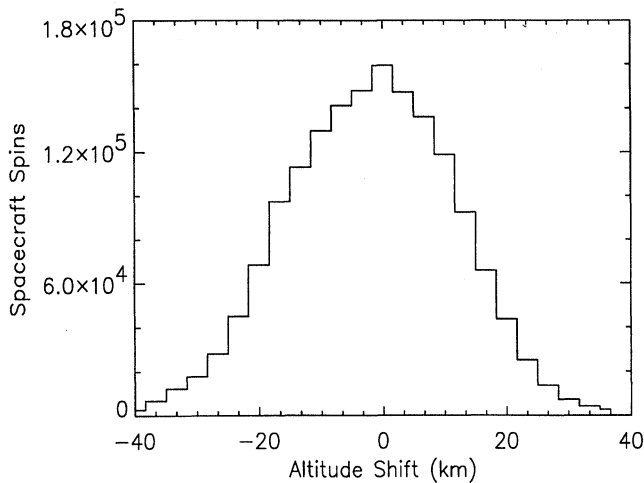


Figure 7. A histogram of the initial altitude shift to 53 km for one million observations. The full width at half maximum indicates the HCIs on SNOE have a ± 20 km error in altitude registration.

The above shift is a preliminary estimate; each UVS profile still needs to be analyzed to determine the exact altitude range measured. The true altitude range is determined by performing a correlation of the data to the model for each profile measured. The data and model are interpolated onto a 1/3 km altitude grid. The data are systematically shifted in altitude in 1/3 km steps over a range of ± 3 km and fitted to the model. The quality of the fit is determined by calculating the correlation coefficient. The correlation coefficient is represented by r :

$$r = \frac{\sum (x_i - \bar{x})(y_i - \bar{y})}{\left[\sum (x_i - \bar{x})^2 \sum (y_i - \bar{y})^2 \right]^{1/2}}. \quad (10)$$

The value of r lies somewhere between -1 and 1 . If r is close to -1 or 1 , then the data sets are linearly related; however, if r is

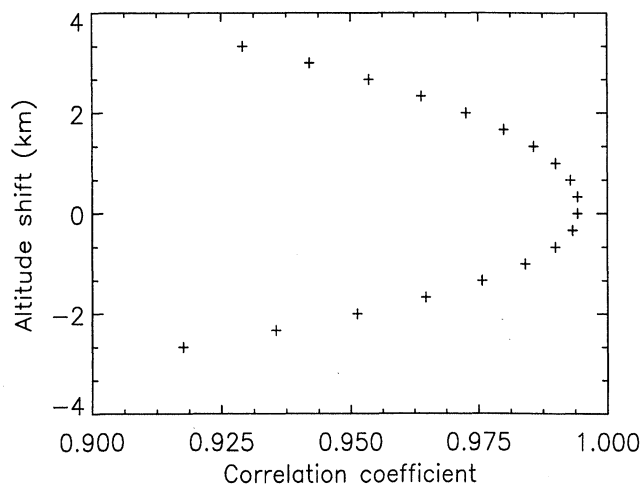


Figure 8. The correlation coefficient for each 1/3 km shift in altitude for one UVS profile. The correlation coefficient is usually > 0.98 when the shift in altitude is the correct amount.

close to 0, then the data sets are uncorrelated [Taylor, 1982]. The correlation coefficient is determined for each shift in altitude. The desired altitude shift is determined when the correlation coefficient is closest to 1. Figure 8 illustrates the change in correlation coefficient for the systematic shift in altitude for one UVS profile. The shifted profile that best correlates with the model profile determines the correct shift in altitude; however, the correlation coefficients shown in Figure 8 are all close to 1. The model and data correlate well with 90% of the observations having a correlation coefficient higher than 0.98. Referencing Figure 8, a correlation coefficient ~ 0.98 corresponds to a shift in altitude of 1 km. To ensure that the uncertainty due to the altitude shift component of the procedure is 1 km, all profiles with correlation coefficients < 0.98 are not used.

In the months of the southern PMC season a correlation coefficient < 0.90 is usually an indicator that a PMC with scatter brightness larger than the Rayleigh-scattering peak has been detected in the data as shown in Figure 9. In the Southern Hemisphere, 5% of observed clouds have $SR > 20$, and as illustrated in Figure 9, the PMC scatter peak has a higher count rate than the Rayleigh peak. When this occurs, it causes the algorithm to fit the model to the cloud profile instead of to the Rayleigh-scattering profile. To correct this, the algorithm is designed to look for the Rayleigh-scattering peak below the PMC and to redetermine the correct altitude shift and correlation coefficient.

The errors contributing to the accuracy of the altitude scale are from the error due to the ozone model of ± 1 km, the random error of ± 1 km determined from the correlation coefficient, and the PMC error of ± 0.5 km. The initial altitude shift to 53 km, described above, eliminates the contribution of the HCI errors. The precision of the resulting altitude determination is the RMS of the three contributing errors, which is ~ 1.5 km. This method of altitude determination provides an acceptable accuracy for the UVS data analysis.

7. Conclusion

The Rayleigh-scattering profile has successfully been used to register the SNOE UVS atmospheric emission profiles in altitude

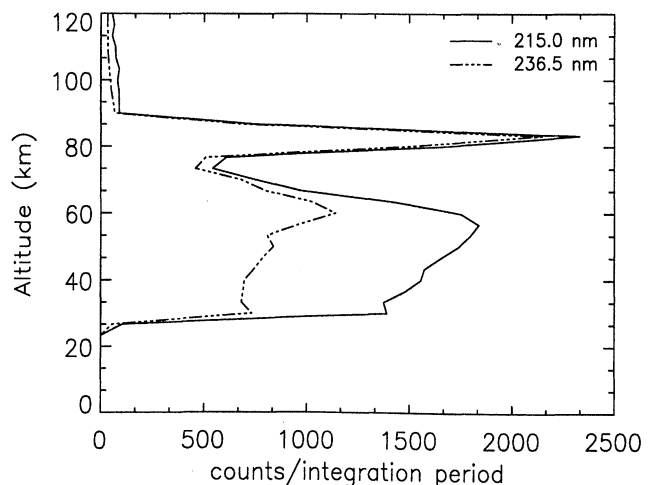


Figure 9. UVS data for both channels with a PMC in the field of view. The PMC occurs around 85 km, while the Rayleigh peak occurs around 53 km for the 215.0 nm channel and around 60 km for the 236.5 nm channel.

to a precision of 1.5 km. The altitude registration was achieved by comparing each measured profile to a modeled Rayleigh-scattering profile. The measured profiles were systematically shifted in small altitude increments and fitted to the model profile using a least squares technique. The quality of the fit determined the correct shift in altitude. The sources of error in this analysis are from the inputs to the Rayleigh-scattering model. The largest source of error is the seasonal and latitudinal distribution of ozone. It was shown that systematically varying the concentration of ozone by 20% caused the altitude of the peak to move only by 1 km.

Acknowledgments. The Student Nitric Oxide Explorer mission has been managed for the National Aeronautics and Space Administration by the Universities Space Research Association. We thank Gary Thomas for his guidance in the development of the radiance model.

Janet G. Luhmann thanks the referees for their assistance in evaluating this paper.

References

- Bailey, S. M., C. A. Barth, M. J. Erickson, R. A. Kohnert, A. W. Merkel, E. M. Rodgers, S. C. Solomon, S. D. Straight, and J. E. Vian, Science instrumentation for the Nitric Oxide Explorer, *Proc. SPIE Int. Soc. Opt. Engr.*, 2830, 264-273, 1996.
- Bates, D. R., Rayleigh scattering by air, *Planet Space Sci.*, 32, 785-790, 1984.
- Chapman, S., The Absorption and dissociative or ionizing effect of monochromatic radiation in the atmosphere on a rotating Earth, *Proc. R. Soc., London*, 43, 483-501, 1931.
- Cowley, J. R., and G. M. Lawrence, Earth limb altitude determination for the Solar Mesosphere Explorer, paper presented at 21st AIAA Aerospace Sciences Meeting, Am. Inst. of Aeronaut. and Astronaut., Reno, Nevada, January 10-13, 1983.
- DeMore, W. B., S. P. Sander, D. M. Golden, R. F. Hampson, M. J. Kurylo, C. J. Howard, A. R. Ravishankara, C. E. Kolb, and M. J. Molina, Chemical kinetics and photochemical data for use in stratospheric modeling: Evaluation number 12, *JPL Publ.*, 97-4, 1997.
- Eparvier, F. G., and C. A. Barth, Self absorption theory applied to rocket measurements of the nitric oxide (1,0) gamma-band in the daytime thermosphere, *J. Geophys. Res.*, 97, 13,723-13,731, 1992.
- Fitzmaurice, J. A., Simplification of the Chapman function for atmospheric attenuation, *Appl. Opt.*, 3, p. 640, 1964.
- Hedin, A. E., MSIS-90 thermospheric model, *J. Geophys. Res.*, 96, 1159-1172, 1991.
- Keating, G. M., M. C. Pitts, and D. F. Young, Ozone reference models for the middle atmosphere, COSPAR International Reference Atmosphere: 1986, part II, Middle atmosphere models, *Adv. Space Res.*, 10, (12), 317-355, 1990.
- Keating, G. M., M. C. Pitts, and D. F. Young, Improved ozone reference models for the COSPAR International Reference Atmosphere, *Adv. Space Res.*, 18, (9/10), 11-58, 1996.
- Larson, W. J., and J. R. Wertz, *Space Mission Analysis and Design*, Kluwer Acad., Norwell, Mass., 1992.
- Rusch, D.W., G. H. Mount, C. A. Barth, R. J. Thomas, and M. T. Callan, Solar mesosphere explorer ultraviolet spectrometer: Measurement of ozone in the 1.0 to 0.1 mbar region, *J. Geophys. Res.*, 89, 11,677-11,687, 1984.
- Solomon, S. C., et al., The Student Nitric Oxide Explorer, *Proc. SPIE Int. Soc. Opt. Eng.*, 2810, 121-132 1996.
- Taylor, J. R., *An Introduction to Error Analysis: The Study of Uncertainties in Physical Measurements*, Univ. Sci. Books, Sausalito, CA.
- Thomas, G. E., and K. Stamnes, *Radiative Transfer in the Atmosphere and Ocean*, Cambridge Univ. Press, New York, 1999.
- Thomas, R. J., C. A. Barth, D. W. Rusch, and R. W. Sanders, Solar Mesosphere Explorer near-infrared spectrometer: Measurements of 1.27- μm radiances and the inference of mesospheric ozone, *J. Geophys. Res.*, 89, 9569-9580, 1984.
- Wang, H. J., D. M. Cunnold, L. Froidevaux, and J. M. Russell, A reference model for middle atmospheric ozone in 1992-1993, *J. Geophys. Res.*, 104, 21,629-21,643, 1999.
- Woods, T. N., et al., Validation of the UARS solar ultraviolet irradiances: Comparison with the ATLAS-1, -2 measurements, *J. Geophys. Res.*, 101, 9541-9569, 1996.

C.A. Barth and A.W. Merkel, Laboratory for Atmospheric and Space Physics, University of Colorado, Boulder, CO 80309-0590, USA.
(Aimee.Merkel@jasp.colorado.edu)

S.M. Bailey, Center for Atmospheric Sciences, Hampton University, Hampton, VA 23668, USA.

(Received January 17, 2001; revised August 13, 2001; accepted August 13, 2001.)